Comparative study of the photodeposition of Pt, Au and Pd on pre-sulphated TiO2 for the photocatalytic decomposition of phenol

M. Maicu, , M.C. Hidalgo, G. Colón, J.A. Navío

Instituto de Ciencia de Materiales de Sevilla (ICMS), Consejo Superior de Investigaciones Científicas (CSIC)-Universidad de Sevilla, Américo Vespucio 49, 41092 Sevilla, Spain

Abstract

A comparative study of the photodeposition of Pt, Au and Pd under the same experimental conditions onto pre-sulphated and non-sulphated TiO2 was performed. Morphological and surface characterisation of the samples as well as photocatalytic activity for phenol photooxidation was studied. The influence of sulphate pre-treatment on the deposits size and dispersion onto the TiO2 surface, and photodeposition yields with the different metals were also analysed. The photocatalytic activity of the doped materials was then investigated, observing that catalytic behaviour can be correlated to physical characteristics of the samples determined by (XRD) X-ray diffraction, (XPS) X-ray photoelectron spectroscopy, (XRF) X-ray fluorescence spectrometry and (TEM) transmission electron microscopy.

Sulphate pre-treatment was found to influence both the level of dispersion and the size of metal clusters on the TiO2 surface. Sulphation and metallisation of samples was found to produce a synergistic enhancement in photoactivity for the degradation of phenol. The photoactivity of the catalysts with respect to the doped metal species was ordered Pt > Pd > Au.

Keywords

Photocatalysis; Sulphated TiO2; Photodeposition; Phenol oxidation; Metal dispersion; Pt–TiO2; Au-TiO2; Pd–TiO2

1. Introduction

The heterogeneous photocatalytic decomposition of organic compounds using TiO2 semiconductor materials as catalysts has often been successfully applied in the treatment of contaminated water and air streams [1], [2], [3] and [4]. Amongst the large band-gap semiconductors investigated as photocatalysts in such processes, TiO2 stands out due to its high photosensitivity, non-toxicity, stability and commercial availability. However, despite these desirable properties, several drawbacks limit the practicality of its application. The band-gap of TiO2 (∼3.23 eV for the anatase form and ∼3.02 eV for the rutile form) corresponds to an adsorption band between 380 and 410 nm, meaning that solar light (composed of only ∼5% UV radiation) cannot be utilised to activate such photocatalytic processes. Additionally, the fast recombination rate of the generated charge carriers combined with a slow transfer rate of electrons to oxygen also limits the efficiency of this photocatalyst.

Noble metal doping of TiO2 materials is one strategy that has been employed in order to improve the efficiency of such photocatalysts. Significant enhancements in activity have been reported in TiO2 materials modified by the surface deposition of Pt, Au and Pd [5], [6], [7], [8],

[9], [10], [11], [12] and [13]. The effect of this metallisation on the photocatalytic activity of TiO2 has caused some controversy in literature, with some of the reported experimental results appearing contradictories. The enhancement (or not) of the photocatalytic activity of TiO2 by metal deposition seems to be highly dependent on the substrate to be degraded as well as on the properties and charge of the metal deposits [5] and [11].

Previously, we reported that pre-treatment of TiO2 with sulphuric acid notably enhances the photoactivity of the resultant semiconductor in the oxidation of phenol [14] and [15]. Sulphation shields the TiO2 surface area against sintering, stabilising the anatase crystalline form until calcination temperatures as high as 700 °C and producing at the same time a highly defective surface. This results from the creation of oxygen vacancies via a dehydroxylation process during calcination. In regard to this, nonstoichiometry has been reported to influence the adsorption energy of Au and Pt on TiO2, also altering significantly the electronic structure of the metal adlayers. Thus, oxygen vacancies have been proved to be preferential sites for metal adsorption. This leads to a better charge-transfer between metal and semiconductor with a consequent increase in the effectiveness of charge separation and therefore in the efficiency of photocatalysis [16], [17] and [18].

In this study, sol–gel TiO2 samples doped with photodeposited Pt, Au or Pd are studied. The photocatalytic behaviours of the samples are compared taking into account the diverse nature of the metals deposited using identical conditions. The photodeposition yields of the different metals are also investigated. Additionally, the effect of sulphate pre-treatment on the size, dispersion and surface properties of metal deposits is studied. Finally, the effect of the metal deposits on photoactivity is evaluated and related to the physical characteristics of the catalyst materials.

2. Experimental

2.1. Catalyst preparation

The TiO2 employed in this study was prepared as follows: titanium tetraisopropoxide (Aldrich, 97%) in isopropanol solution (1.6 M) was hydrolysed by the addition of distilled water (volume ratio: isopropanol/water 1:1). The resulting precipitate was subsequently filtered, washed twice with distilled water and dried at 110 °C overnight.

Non-sulphated TiO2 (TiO2ns) was obtained by calcining a portion of the dried precipitate at 500 °C for 2 h. Sulphated TiO2 (TiO2s) was prepared by immersing the precipitate in 1 M sulphuric acid solution for 1 h. The precipitate was then filtered again, dried at 110 °C overnight and calcined at 700 °C for 2 h, following the same procedure used in our previous work [15]. The calcination temperatures described for both materials have previously shown to produce samples with optimum photocatalytic activity in the degradation of phenol. In this regard, TiO2ns should not be calcined at 700 °C as this temperature leads to a nearly complete loss of the surface area and total rutilisation of the material, and consequently to a very poor photocatalytic activity. TiO2s should not be calcined at 500 °C as this temperature is not high enough to eliminate sulphate groups from the TiO2 surface, leading equally to a poor photocatalytic activity [14] and [15].

Metal doping of the calcined TiO2 samples was performed by photodeposition, following a modified version of a previously reported method [8]. Pt, Au and Pd doping was achieved using hexachloroplatinic(IV) acid (H2PtCl6, Merck 40% Pt), tetrachloroauric acid (HAuCl4, Sigma–Aldrich, 99.9+%) and palladium(II) chloride (PdCl2, Sigma–Aldrich, 99.9+%) respectively as precursors. Solutions of the appropriate concentrations of metal chloride (corresponding to a 0.5–2 wt.% metal loading) in distilled water were prepared and mixed with suspensions of the TiO2 in distilled water (5 g TiO2 L−1), adding isopropanol as sacrificial donor (0.3 M final concentration). Photodeposition was performed by illuminating the suspensions for 6 h with a medium pressure mercury lamp (400 W) of photon flux ca. 2.6 × 10−7 Einstein s−1 L−1 in the <400 nm region while maintaining continuous nitrogen purging. The product was then recovered by filtration, and dried at 110 °C overnight. Some selected metallised samples were independently prepared and analysed twice, with both morphological properties of the metal deposits and photocatalytic behaviour found to be reproducible. As the maximum photocatalytic activity was achieved in all cases at a nominal metal content comprised between 1 and 2 wt.%, for the sake of brevity only the results obtained by the characterisation of samples containing 1.5 wt.% of metal will be shown in order to compare the three metal/TiO2 systems.

From this point onward samples will be annotated TiO2ns or TiO2s (corresponding to the non-sulphated and pre-sulphated materials respectively) followed by the chemical symbol of the photodeposited metal and the wt.% loading, e.g., “TiO2s–Pt1.5” refers to sulphated TiO2 platinised with 1.5 wt.% loading.

2.2. Characterisation of the catalysts

Phase composition and the degree of crystallinity in the samples were determined by X-ray diffraction (XRD). XRD patterns were recorded on a Siemens D-501 diffractometer equipped with a Ni filter and graphite monochromator using Cu Kα radiation (λ = 1.5418 Å). Crystallite sizes in the different phases were estimated from line broadening of the corresponding X-ray diffraction peaks by using the Scherrer equation. Peaks were fitted using the Voigt function.

The morphology of the samples and the dispersion and size of surface metal deposits were studied by transmission electron microscopy (TEM) using a Philips CM 200 instrument. The microscope was equipped with a top-entry holder and ion pumping system, operating at 200 kV and employing a nominal structural resolution of 0.21 nm. Samples were prepared by dispersing the powders in ethanol using ultrasound and dropping onto a carbon grid.

Surface characterisation by X-ray photoelectron spectroscopy (XPS) was conducted on a Leybold-Heraeus LHS-10 spectrometer, working with constant pass energy of 50 eV. The spectrometer main chamber was maintained at a pressure <2 × 10−9 Torr, and the machine was equipped with an EA-200 MCD hemispherical electron analyser with a dual X-ray source of Al Kα (hv) 1486.6 eV at 120 W and 30 mA. The carbon 1 s signal (284.6 eV) was used as the internal energy reference in all the measurements. Samples were outgassed in the prechamber of the instrument at 150 °C up to a pressure <2 × 10−8 Torr to remove chemisorbed water from their surfaces.

Total metal content of the samples was determined by X-ray fluorescence spectrometry (XRF) in a Panalytical Axios sequential spectrophotometer equipped with a rhodium tube radiation source. XRF measurements were performed on pressed pellets (the sample incorporated in 10 wt.% wax).

BET surface area and porosity measurements were carried out by N2 adsorption at 77 K using a Micromeritics ASAP 2010 instrument.

Light absorption properties of the samples were studied by UV–vis spectroscopy. UV–vis spectra were recorded on a Varian Cary 100 spectrometer equipped with an integrating sphere using BaSO4 as reference. Both absorbance and diffuse reflectance spectra were recorded for all samples and the Kubelka–Munk function, F(R∞), was applied to obtain a magnitude proportional to the extinction coefficient. Band-gaps were calculated by the Kubelka–Munk function, following the method proposed by Tandom and Gupta [19].

2.3. Photocatalytic runs

The photocatalytic activity of the samples was evaluated in the reaction of phenol oxidation. Suspensions of the samples (1 g L−1) in aqueous phenol solution (50 ppm) were placed in a batch reactor (200 mL) and illuminated for 2 h through a UV-transparent Plexiglas top window (threshold absorption at 250 nm) by an Osram Ultra-Vitalux lamp (300 W) with a sun-like radiation spectrum and a main emission line in the UVA range at 365 nm. The intensity of the incident UVA light on the solution was determined to be approximately 95 W m−2 using a PMA 2200 UVA photometer (Solar Light Co.). Magnetic stirring and a constant flow of oxygen maintained the homogeneous suspension of catalyst in the solution. Prior to illumination, catalyst-substrate equilibration was ensured by stirring the suspension for 20 min in the dark. The evolution of the phenol concentration was measured by UV–vis spectrometry, following the 270 nm characteristic band of phenol. The activity of the catalysts was determined from the initial degradation rate (30 min), since zero-order kinetics are followed at this stage. For the metallised samples an “enhancement factor” (Ef), defined as the quotient between the rate of the photoprocess over the metallised catalyst and the rate of the same photoprocess over the non-metallised catalyst [11], was also calculated.

No observable change in the initial phenol concentration was noted in blank experiments where no catalyst was used, both in the presence and absence of illumination.

3. Results

3.1. Characterisation of the samples

Crystalline phase composition of the samples was studied by XRD and XRD patterns for non-sulphated and pre-sulphated TiO2, both without and with 1.5 wt.% photodeposited metal (Pt, Au and Pd), are shown in Fig. 1. For each metal/TiO2 system the sulphate-pretreated series was found to consist only of the anatase form, while the non-sulphated materials were also composed of a trace level of brookite, indicated by the small peak at diffraction angles of 2θ ∼31° corresponding to the (1 2 1) plane. The addition of noble metals did not alter the phase composition of the TiO2. Neither the position nor the width of the peaks changed significantly after deposition, which indicates that there was no distortion of the original TiO2 structure.

However, in all series some small peaks associated with the metal deposits were observable. In the Pt/TiO2 materials, two reflections at diffraction angles of 2θ ∼40° and 2θ ∼46° assignable respectively to diffraction on the (1 1 1) and (2 0 0) planes of metallic platinum were recorded. Likewise, the diffraction patterns of Au/TiO2 materials showed two peaks, located at 2θ ∼45° and 2θ ∼65° respectively, corresponding to the (2 0 0) and (2 2 0) planes of Au0; and in the Pd/TiO2 samples a small peak at 2θ ∼30° is due to diffraction by the (1 1 1) plane of Pd0. Anatase crystallite sizes were estimated by the Scherrer equation and the results obtained are presented in Table 1. Particles of non-sulphated materials were found to range in size from 15 to 19 nm, while pre-sulphated samples had crystallite sizes of around 30 nm independently of the presence of photodeposited metal.

Regarding BET surface area values, amongst the metallised materials the non-sulphated samples exhibited BET surface areas of 55 ± 5 m2 g−1 while for the pre-sulphated ones areas of 25 ± 5 m2 g−1 were found. Photodeposition of the different metals did not appreciably affect the surface area of the TiO2, the BET values decreasing only slightly in non-sulphated samples. The lower surface area observed for the sulphated TiO2 is ascribable to the higher calcination temperature used in its preparation. Despite this, we have previously shown that pre-treatment with sulphuric acid clearly has the effect of stabilising both the TiO2 surface against sintering and the anatase crystal form up to high calcination temperatures (700 °C), as demonstrated by the BET surface area of only 5 m2 g−1 observed for non-sulphated TiO2 calcined at 700 °C [15]. These results can be related to the differences observed between the non-sulphated and pre-sulphated samples in terms of anatase crystallite size since samples with the higher surface areas are composed of smaller TiO2 particles.

Light absorption properties of the materials were studied by UV–vis spectroscopy and the diffuse reflectance spectra of selected samples, both undoped and doped with 1.5 wt.% of Pt, Au and Pd, are illustrated in Fig. 2. Comparison of the spectra of pre-sulphated and non-sulphated samples shows up no notable differences in the UV region, with the strong, broad absorption observed below ca. 400 nm ascribable to charge-transfer from the valence to the conduction band of the TiO2[20]. However, in the visible region of the spectra, the metal-loaded materials show characteristic absorption patterns due to the colouration of the powders (dark grey for Pt and Pd, and violet for Au). In the Pt-doped materials, three small peaks located at ca. 450, 500 and 700 nm can be attributed to the Pt clusters. The intensity of these signals is higher in the sulphated materials. Similarly, peaks at ca. 470, 530 and 710 nm are observable in the reflectance spectra of the Pd/TiO2 samples. The absorption of visible light by metallised samples has been ascribed to low-energy transitions between the valence band of TiO2 and localised energy levels introduced to the band-gap by deposited metal clusters [12]. The non-constant nature of absorption in the visible region is probably due to the variable size of metal deposits, which leads to multiple signals at wavelengths corresponding to the various permitted electronic transitions. In contrast, the reflectance spectra of the Au/TiO2 samples show only a single absorption, corresponding to the characteristic gold surface plasmon with a maximum at 540 nm. A surface plasmon resonance is a unique feature of noble metals such as gold and silver and it is originated from the collective oscillations of the electrons at the surface of the nanoparticles. A strong dependence of the bandwidth and position of the plasmon signal on the size of the deposited gold nanoparticles has been demonstrated experimentally. The bandwidth has been found to increase as the particle size

decreases for gold clusters having diameters below 25 nm, and to increase as the particle size increases for diameters greater than 25 nm. The position of the absorption maximum of the resonance plasmon is also dependent on the particle size, with red-shift observed for increasing diameters up to 25 nm and both red- and blue-shift for smaller metal clusters [21] and [22]. In the samples studied here however, a relationship between the size of the gold deposits and the position and bandwidth of the plasmon is not apparent, probably due to the wide ranging diameters of the photodeposited gold particles, as it will be shown in the TEM study discussed below. Despite the absorption properties observed for the different modified TiO2, a similar band-gap between 3.2 and 3.3 eV was found for all samples.

Size and dispersion of metal deposits in the doped samples was investigated by TEM. Selected micrographs of the metal/TiO2 samples are shown in Fig. 3. As it can be observed in Fig. 3(a) and (d), photodeposited Pt particles are always found to be spherical in shape, although higher dispersions and smaller average deposit sizes are observed in the sulphated TiO2. In Fig. 4(a), particle size distribution for the metal in the Pt/TiO2 system is presented, estimated by measuring dimensions of visible platinum particles across a large number of TEM micrographs. It can be seen that for the non-sulphated TiO2 most of the Pt deposits have diameters ranging from 3 to 6 nm, while for the pre-sulphated material the average particle size is smaller, having more than 50% of the platinum particles an average diameter in the range of 2–4 nm.

For the Au/TiO2 system, photodeposited gold show poor homogeneity and dispersion of deposits with some areas of the TiO2 surface having a high density of Au particles and others being relatively empty, as it can be seen in the selected micrographs showed in Fig. 3(b) and (e). Additionally, Au particles deposited via this method are irregularly sized, varying from around 10 nm to more than 100 nm in diameter. Due to the high heterogeneity in size, counting metal particles was not possible for this system.

Contrary to the observations made from TEM analysis of the metal clusters in Pt and Au doped samples, Pd particles are actually smaller and more regularly sized and shaped in the non-sulphated samples, as it can be seen in Fig. 3(c) and (f). The estimation of Pd average particle size presented in Fig. 5(b) shows that Pd particles deposited on non-sulphated TiO2 have diameters ranging from approximately 3 to 7 nm while on the pre-sulphated sample the average size is higher with particles ranging from 4 to 10 nm.

The total metal content of the samples was determined by XRF and the results are shown in Table 1. Fig. 5 shows the nominal metal content vs. total metal content (measured by XRF) for the sulphated and non-sulphated samples for all three metal/TiO2 series. From this the efficiency of the photodeposition method was evaluated observing differences between the three noble metals. It was found that, under these experimental conditions, photodeposition is an effective means of depositing Pt onto TiO2 surfaces, being the bulk content of platinum in all cases only slightly less than the theoretical content (%Pt(XRF) $\simeq$ %Pt(nominal)). The yield in the photodeposition of Au was slightly lower than for Pt, as shown by Fig. 5, and fell significantly, to only $\sim$50%, in the case of Pd.

XRF measurements were also performed in order to evaluate the possible presence of residual Cl on the photocatalysts surface due to the use of Cl-containing metal precursors. The results

showed in all non-sulphated samples negligible contents of Cl (≤0.1%) and no traces of this element in the sulphated and calcined materials.

All samples were studied by XPS. The binding energy for the Ti 2p3/2 peaks (data not shown) is approximately 458.5 eV in every case, and this can be attributed to Ti4+ in the TiO2 lattice. The O 1s peak is observed in all samples at around 530.0 eV, the value corresponding to the binding energy of lattice oxygen. From these data, O/Ti ratios were calculated for each sample and the values are shown in Table 1. In some of the samples this ratio is lower than the stoichiometric value (O/Ti = 2), indicating the presence of oxygen vacancies on the surface of the materials. In general, sulphated TiO2 presents a lower O/Ti ratio that non-sulphated TiO2, which indicates that the amount of oxygen vacancies is higher in the former samples. For Pt/TiO2 and Pd/TiO2 samples, both the sulphated and non-sulphated samples possess O/Ti ratios closer to the stoichiometric value of 2 after metallisation, indicating that many of the vacancies disappear during the photodeposition process. In contrast, photodeposition of Au onto both sulphated and non-sulphated TiO2 did not lead to the annihilation of the vacancies, keeping these samples still a low O/Ti ratio. Au is preferentially deposited on deficient surfaces, therefore it could be assumed that Au clusters would stabilise O vacancies during photo reduction.

In all sulphated samples, XPS analysis of the S 2p region produced no signal, indicating that the levels of S on the materials surface following calcination at 700 °C were negligible, according to previous observations [14].

XPS also allowed the determination of the oxidation state of the Pt, Au and Pd. With respect to the photocatalytic properties of the materials this information is important since it is believed that the metallic state (M0) induces the greater enhancements in the photocatalytic activity of TiO2 by creating a Schottky junction between metal and semiconductor. The metal particle acts as a sink for photogenerated electrons, reducing the rate of their recombination with holes [23] and [24]. Fig. 6(a) shows the XPS spectra in the Pt 4f region for sulphated and non-sulphated platinised TiO2. The Pt signal consists of three pairs of doublets, the most intense (located at ca. 70.2 and 73.6 eV) corresponding to metallic Pt. The other two pairs of peaks appearing at 71.5 and 73.1 eV correspond respectively to the 4f7/2 signals of Pt2+ and Pt4+. It can be therefore concluded that the platinum was photodeposited mainly as Pt0, with a small amount of Pt2+ and Pt4+.

The Au 4f region of the Au/TiO2 samples is shown in Fig. 6(b). The Au signal takes the form of a doublet at a binding energy of 83.1 and 86.8 eV, corresponding to the Au 4f7/2 and Au 4f5/2 signals respectively, and can be assigned to metallic gold (Au0). No peaks or shoulders are observable at higher binding energies and it can hence be concluded that the photodeposition has succeeded in completely reducing the Au, leaving no detectable trace of Au+ or Au3+.

Fig. 6(c) shows the 3d region of the XPS spectra for the palladium-doped materials. The palladium signal consists of a doublet with the two peaks corresponding to Pd 3d3/2 and Pd 3d5/2. The binding energy of Pd0 is known to be approximately 334 eV [25], while the peaks corresponding to the metal oxidation states Pd2+ and Pd4+ are located at approximately 336.4 eV for PdO and at approximately 337.6 eV for PdO2. In Fig. 6(c), the Pd 3d5/2 signal is observed at Eg ≃ 334.9 eV for the non-sulphated sample and Eg ≃ 334.6 eV for the sulphated

one, indicating that the metal on the TiO2 surface is mainly metallic (Pd0), in agreement with the XRD study that was previously discussed. However, both components of the doublet (Pd 3d5/2 and Pd 3d3/2) appear asymmetric due to a shoulder at higher binding energies. This feature is especially pronounced in the non-sulphated sample, and may be due to the presence of small amount of metal in higher oxidation states (Pd2+ and/or Pd4+).

3.2. Photocatalytic activity

The photocatalytic activity of both pre-sulphated and non-sulphated metal/TiO2 samples was evaluated in the reaction of photooxidation of phenol. In Fig. 7 the phenol degradation profiles over all samples are shown. As it can be seen, metallisation of both non-sulphated and pre-sulphated TiO2 resulted in a great enhancement of the photocatalytic activity in every case, with the only exception of the TiO2ns–Au system. It appears also clear that in each series the most active photocatalysts in absolute value were the platinised samples. In fact, total degradation of phenol was reached within only 60 min using these materials as catalysts. The photooxidation of phenol was almost complete after about 120 min when the photodegradation was conducted over the other catalysts. It is worth to notice that in any case the profiles of phenol degradation did not show any important deceleration at prolonged illumination times, suggesting that no resistant intermediates were formed during the reaction.

Taking into account the different surface area of the samples in both series, initial decomposition rates for this model reaction, normalised per surface unit of catalyst, are shown in Fig. 8. Here the enhancement factors (Ef) of the metallised samples for this reaction are also reported. As it can be observed, for all systems, sulphated TiO2 presented a higher activity than non-sulphated TiO2.

With the deposition of Pt, a high enhancement of the activity of TiO2 was observed, especially for the sulphated TiO2 which presented an Ef of 2.46. Au and Pd deposition on sulphated TiO2 produced also an improvement of the activity, with Ef 1.21 and 1.33 respectively, although the enhancements were not so high as for the case of Pt deposition. For the three metals, the increase of the photocatalytic activity was higher when the deposition was performed on sulphated TiO2. Moreover, as it has been commented above, the addition of Au to non-sulphated TiO2 produced a negative effect on the activity, decreasing the rate of photodegradation of phenol with respect to the non-metallised TiO2 (Ef < 1).

In summary, best photocatalyst for phenol oxidation resulted to be the platinised sulphated TiO2, being the order for the photocatalytic improvement with respect to the doped metal species Pt > Pd > Au.

4. Discussion

The photoactivity of TiO2 for phenol oxidation was greatly enhanced by sulphate pre-treatment. Characterisation of these materials reported elsewhere has demonstrated that pre-treatment of TiO2 with sulphuric acid followed by calcination at 700 °C results in both structural surface area stabilisation and the creation of a significant number of subsurface vacancies [14] and [15]. Implicit in the formation of these stabilised vacancies during the

calcination is the concurrent creation of intermediate states in the band-gap of the semiconductor, both enhancing the photon absorbance, and acting as traps for electrons. The latter inhibits the recombination of photogenerated charges, improving their diffusion to the surface and consequently enhancing the photocatalytic activity of the material.

The Pt-doped samples showed significantly higher photocatalytic activity than the non Pt-doped counterparts. Noble metal nanoparticles deposited on the TiO2 surface are known to act as effective traps for photogenerated electrons due to the formation of a Schottky barrier at the metal-semiconductor contact. These electrons improve the rate of oxygen reduction and inhibit the electron–hole recombination [8] and [10]. In theory, the efficiency of metal deposits as electron traps should improve with higher dispersion and lower particle size, as was observed in this study for platinum photodeposition, particularly for the sulphated material. This infers that the lower particle size and higher dispersion of platinum observed by TEM on the pre-sulphated material contributed to a higher photocatalytic activity in the photooxidation of phenol than in the non-sulphated catalyst. These results also demonstrate a synergistic enhancement in catalytic activity in sol–gel TiO2 which has been both sulphate treated and Pt-doped [6]. Beside, it has also been reported a larger adsorption energy of Pt over nonstequiometric TiO2 surfaces than over stequiometric ones [17]. As XPS results have shown, sulphated TiO2 has a higher amount of surface oxygen vacancies and therefore Pt particles would present a stronger adsorption and improved electronic contact over this material, leading to a more effective trapping of electrons and inhibiting to a higher degree electron–hole recombination.

Regarding Au/TiO2 systems, some improvement in the photocatalytic activity of TiO2 was also achieved by surface deposition of Au nanoparticles on pre-sulphated materials subjected to high temperature calcination (700 °C). The greater enhancement of catalytic activity in the pre-sulphated samples was also ascribed to the stronger bonding, improved electronic junction and better communication between the Au clusters and the TiO2 surface on the more highly defective surfaces presented by the sulphated material [7], [16], [17] and [18], effects more marked for this system than for the case of Pt. As we have seen, this would increase the efficiency of charge separation and thus the efficiency of photocatalytic process.

Surprisingly however, for the non-sulphated sample the activity decreased with the deposition of metal, being the corresponding Ef lower than 1. This is probably due to shadowing and blocking of the TiO2 active sites by bulky and otherwise ineffective Au particles in these samples.

The difference between the photocatalytic behaviours of Au and Pt-doped catalysts prepared by photodeposition of the metal on non-sulphated TiO2 is of considerable interest. Photodeposition of Pt or Au begins with the electrostatic interaction between the TiO2 particles and the dissolved metal complex ($AuCl_4^-$, $AuOHCl_3^-$, $PtCl_6^{2-}$), leading to the adsorption of the salt precursor on the surface of the semiconductor. The nature and concentration of the adsorbed metal precursor, as well as the final content of Pt and Au following the photoreduction process, depends on several factors, such as the initial salt concentration, the pH, the temperature, the type of reducing agent and the duration and intensity of illumination. In this study all samples were prepared in identical fashion in order to

allow direct comparison of results. However, a study by Bamwenda et al. [26] has compared the photocatalytic activity of Pt/TiO2 and Au/TiO2 systems prepared, amongst others methods, by photodeposition of the same metal precursors as employed in this study and showed that the optimum conditions for photodeposition of the two metals are actually distinct, being the pH of the solution apparently a crucial parameter. In their study the photodeposition of Pt was carried out at a pH 4 (equal to the pH of the precursor solution employed in this study) while photodeposition of Au was carried out at pH 7. The pH most probably affects absorption of precursors onto the TiO2 surface due to its influence on the superficial charge, with optimum absorption occurring at the cited pH values. In this study the photodeposition of both metals was carried out at pH 4, which may explain the observed discrepancy between the yield and the size and dispersion of the metal clusters. The conditions employed in the preparation of the Au doped catalyst are therefore probably responsible for the inferior electronic contact between the photodeposited gold and the TiO2 due to poorer adsorption of clusters on the semiconductor surface compared to the platinum doped material, specially in non-sulphated TiO2 which contains a low amount of vacancies. Additionally, this would also lead to the formation of Au-islands poorly distributed with large and irregular dimensions, as it has been observed by the TEM study of the samples. The inferior photocatalytic efficiency of the Au-doped catalysts compared to the Pt-doped counterparts is likely to be a result of a combination of these factors.

Fig. 7 and Fig. 8 also show the results obtained in the photodecomposition of phenol over the Pd loaded TiO2. Similar to the other metal/TiO2 catalysts, photoefficiency was found to be higher in the pre-sulphated samples. Despite of the lower metal yield in the Pd deposition compared to Au, a greater increase in the photocatalytic activity was observed in the Pd doped catalysts, as illustrated by comparison of the Ef. From these results we can conclude that although the photoactivity of metal-doped TiO2 is strongly dependent on the superficial metal loading, this is not the only factor to take into account. The interaction between the semiconductor and the metal clusters is also crucial, as was previously discussed. Consequently, although photochemical reduction of Pd over the TiO2 surface did not result in complete reduction of the precursor, there was stronger bonding and thus better electronic contact between the metal and semiconductor than in the Au-doped TiO2. Platinum group metals (particularly Pt and Pd) can act as traps for photogenerated electrons, reducing the rate of electron–hole recombination, behaving as wells from which electrons can be subsequently transferred to oxygen and thus increasing the efficiency of photocatalysis [27]. Another important factor to consider which differs between the Pd and Au loaded materials is the size and dispersion of metal particles. Pd deposits were shown to have mean diameters of 4–6 nm on the non-sulphated samples and 5–7 nm on the sulphate-pretreated samples, size distribution being much smaller than in the Au-TiO2 catalysts. However, both the mean diameters and size distribution of particles were higher than those observed for the Pt-doped samples which also showed the highest photocatalytic activities in the photooxidation of phenol. In this case, pH may not appear to be so important parameter in the photodeposition of Pd, with pH control not apparently considered in sample preparations by various researchers using similar techniques [28] and [29]. However, Zhang et al. [30] demonstrated that the morphology and size of photodeposited Pd particles were strongly linked to the pH of the solution. They observed that increasing pH up to 10–13 led to smaller and more uniformly

distributed metal deposits, attributed to changes in the superficial charge of TiO2 and the adsorption of Pd ions. These factors probably affect both nucleation and growth kinetics, assumed to be determining parameters in the final morphology of deposits. The acidic conditions employed during the preparation of our samples (pH of reaction medium ∼4 and pre-treatment of TiO2 with H2SO4), would therefore explain the different morphology observed by TEM for the platinum and palladium-doped catalysts and also explain why for the Pd/TiO2 materials, larger and less homogeneously dispersed metal particles were observed on the pre-sulphated samples, in contrast to observations in the two previous cases.

5. Conclusions

Photodeposition was shown to be a generally efficient method for depositing noble metals onto the surface of TiO2 materials. The highest yields were obtained in the photorreduction of Pt (∼100%) and the lowest for Pd (∼50%), shown by measuring total metal content of samples with XRF.

XRD results demonstrated that the pre-treatment of TiO2 with sulphuric acid clearly stabilises its surface area against sintering and also stabilises the anatase crystal form at higher calcination temperatures than the non-sulphated material. Sulphate pre-treatment of the TiO2 surface also improves the efficiency of metal photodeposition, with better dispersion of the metals and also lower particle size, particularly for Pt. Differences observed in the morphology of the different samples can be attributed to the preparation conditions, particularly the pH of the solution during the photorreduction. The results indicate that optimum conditions exist for each respective photodeposition, giving high adsorption yields and better photocatalytic properties in the resulting catalysts.

The photocatalytic activity of all samples was evaluated in the photooxidation of phenol. Non-sulphated Pt-doped TiO2 showed a significant enhancement in photoefficiency after metal deposition, as illustrated by an Ef of 2.37. Pd deposition resulted in modest improvements in the photoactivity (Ef = 1.17), while photodeposited Au actually resulted in a lowered catalytic activity in comparison to unmodified TiO2, with a calculated Ef of 0.63.

Higher activities were observed with pre-sulphated and metal-doped samples in every case, clearly demonstrating a synergistic enhancement effect by the combination of sulphuric acid treatment with high temperature calcination and metallisation. The highest improvement of the activity for phenol oxidation happened in the platinised sulphated TiO2, with an Ef of 2.46. The photoactivity of the catalysts with respect to the doped metal species was ordered Pt > Pd > Au.

In the metal-loaded systems, enhancements in the activity after sulphating can be directly related to the better dispersion and the reduced size of deposits on the acid treated support. Additionally, the photocatalytic process will be favoured by the stronger bonding and superior electronic junction between the metal deposits, particularly for Au particles, and the more highly defective TiO2 surface of the sulphate-pretreated materials.

Acknowledgements

Financial support by the Spanish Ministerio Ciencia e Innovación (Project Ref. CTQ2008-05961-CO2-01) and Junta de Andalucía (P06-FQM-1406) are acknowledged.

References

[1] V. Augugliaro, M. Litter, L. Palmisano, J. Soria

J. Photochem. Photobiol. C, 7 (2006), pp. 127–144

[2] O. Carp, C.L. Huisman, A. Reller

Prog. Solid State Chem., 32 (2004), pp. 33–177

[3] M. Kitano, M. Matsuoka, M. Ueshima, M. Anpo

Appl. Catal. A, 325 (2007), pp. 1–14

[4] A. Fujishima, X. Zhang, D.A. Tryk

Surf. Sci. Rep., 63 (2008), pp. 515–582

[5] M.C. Hidalgo, M. Maicu, J.A. Navío, G. Colón

Catal. Today, 129 (2007), pp. 43–49

[6] M.C. Hidalgo, M. Maicu, J.A. Navío, G. Colón

Appl. Catal. B, 81 (2008), pp. 49–55

[7] M.C. Hidalgo, M. Maicu, J.A. Navío, G. Colón

J. Phys. Chem. C, 113 (2009), pp. 12840–12847

[8] D. Hufschmidt, D. Bahnemann, J.J. Testa, C.A. Emilio, M.I. Litter

J. Photochem. Photobiol. A, 148 (2002), pp. 223–231

[9] V. Iliev, D. Tomova, L. Bilyarska, G. Tyuliev

J. Mol. Catal. A, 263 (2007), pp. 32–38

[10] V. Iliev, D. Tomova, R. Todorovska, D. Oliver, L. Petrov, D. Todorovsky, M. Uzunova-Bujnova

Appl. Catal. A, 313 (2006), pp. 115–121

[11] S.K. Lee, A. Mills

Platinum Met. Rev., 47 (2003), pp. 61–72

[12] S. Sakthivel, M.V. Shankar, M. Palanichamy, B. Arabindoo, D.W. Bahnemann, V. Murugesan

Water Res., 38 (2004), pp. 3001–3008

[13] Y.Z. Yang, C.H. Chang, H. Idriss

Appl. Catal. B, 67 (2006), pp. 217–222

[14] G. Colón, M.C. Hidalgo, G. Munuera, I. Ferino, M.G. Cutrufello, J.A. Navío

Appl. Catal. B, 63 (2006), pp. 45–59

[15] G. Colón, M.C. Hidalgo, J.A. Navío

Appl. Catal. B, 45 (2003), pp. 39–50

[16] K. Okazaki, Y. Morikawa, S. Tanaka, K. Tanaka, M. Kohyama

Phys. Rev. B, 69 (2004), p. 235404

[17] K. Okazaki, Y. Morikawa, S. Tanaka, K. Tanaka, M. Kohyama

J. Mater. Sci., 40 (2005), pp. 3075–3080

[18] A. Vittadini, A. Selloni

J. Chem. Phys., 117 (2002), pp. 353–361

[19] S.P. Tandom, J.P. Gupta

Phys. Status Solidi, 38 (1970)

[20] H. Gerischer, A. Heller

J. Phys. Chem., 95 (1991), pp. 5261–5267

[21] S. Link, M.A. El-Sayed

J. Phys. Chem. B, 103 (1999), pp. 8410–8426

[22] S. Link, M.A. El-Sayed

J. Phys. Chem. B, 103 (1999), pp. 4212–4217

[23] A. Orlov, D. Jefferson, N. Macleod, R. Lambert

Catal. Lett., 92 (2004), pp. 41–47

[24] V. Subramanian, E.E. Wolf, P.V. Kamat

J. Am. Chem. Soc., 126 (2004), pp. 4943–4950

[25] M.A. Aramendía, V. Borau, J.C. Colmenares, A. Marinas, J.M. Marinas, J.A. Navío, F.J. Urbano

Appl. Catal. B, 80 (2008), pp. 88–97

[26] G.R. Bamwenda, S. Tsubota, T. Nakamura, M. Haruta

J. Photochem. Photobiol. A, 89 (1995), pp. 177–189

[27] A. Mills, S.-K. Lee

Platinum Met. Rev., 47 (2003), pp. 2–12

[28] J. Papp, H.S. Shen, R. Kershaw, K. Dwight, A. Wold

Chem. Mater., 5 (2002), pp. 284–288

[29] Z. Wu

J. Hazard. Mater., 164 (2009), pp. 542–548

[30] F. Zhang

Catal. Today, 93–95 (2004), pp. 645–650

Figure captions

Figure 1. XRD patterns for (a) non-sulphated and (b) sulphated TiO2, displaying undoped samples and samples with 1.5 wt.% photodeposited Pt, Au, and Pd. A: anatase and B: brookite.

Figure 2. UV–vis diffuse reflectance spectra for (a) non-sulphated and (b) sulphated TiO2, displaying undoped samples and samples with 1.5 wt.% photodeposited Pt, Au, and Pd.

Figure 3. Selected TEM micrographs for (a) TiO2ns–Pt (b) TiO2ns–Au (c) TiO2ns–Pd (d) TiO2s–Pt, (e) TiO2s–Au and (f) TiO2s–Pd.

Figure 4. Particle size distribution for (a) Pt and (b) Pd clusters, determined by counting deposits in a large number of TEM micrographs.

Figure 5. Total metal content (measured by XRF) for the sulphated and non-sulphated samples in the three systems: Pt/TiO2, Au/TiO2, Pd/TiO2.

Figure 6. XPS spectra of the (a) Pt 4f, (b) Au 4f and (c) Pd 3d regions for the sulphated and non-sulphated samples with 1.5 wt.% metal doping.

Figure 7. Profiles of phenol degradation over the different non-sulpated (a) and pre-sulphated photocatalysts (b) with the illumination time. [Phenol]0 = 50 mg L−1, V = 0.2 L, [catalyst] = 1 g L−1, I = 95 W m−2.

Figure 8. Initial reaction rates in the decomposition of phenol (mg of phenol degraded per litre per second) normalised per surface area unit of catalyst (m2).

Table 1

Table 1. Summary of characterisation results.

Sample	Anatase crystallite size (nm)	M[a] (wt.%) (XRF)	O/Ti (XPS)
TiO_2ns	17	–	1.89
TiO_2ns–Pt 1.5	19	1.40	1.92
TiO_2ns–Au 1.5	15	1.14	1.75
TiO_2ns–Pd 1.5	17	0.75	2.08
TiO_2s	31	–	1.70
TiO_2s–Pt 1.5	31	1.49	1.95
TiO_2s–Au 1.5	30	0.86	1.76
TiO_2s–Pd 1.5	30	0.95	1.80

[a]M = metals: Pt, Au, Pd.

Figure 1

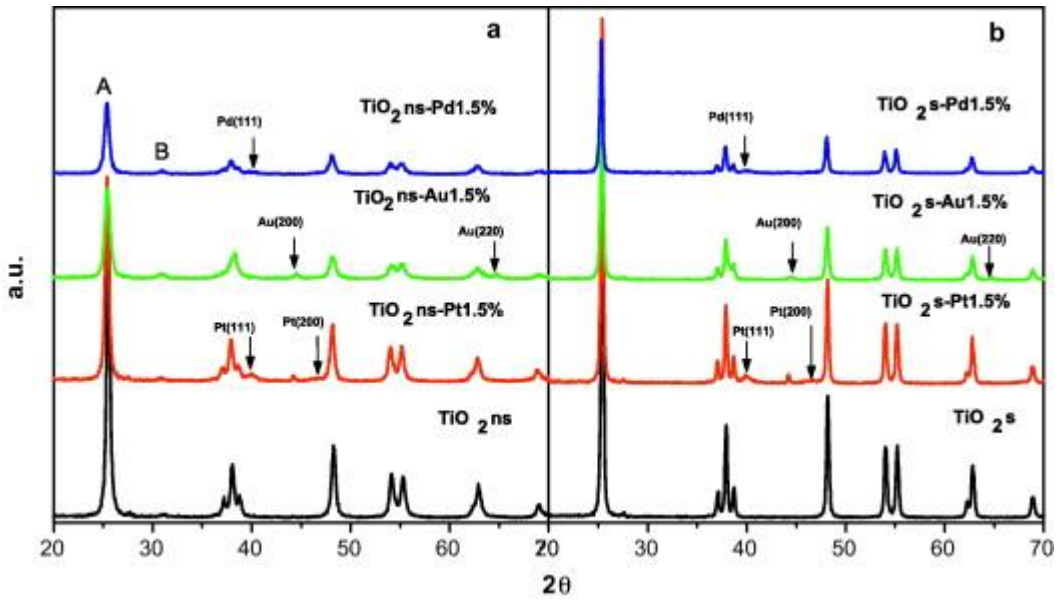
a
b
A
B
Pd(111)
Au(200)
Au(220)
Pt(111)
Pt(200)
TiO2 ns-Pd1.5%
TiO2 ns-Au1.5%
TiO2 ns-Pt1.5%
TiO2 ns
TiO2 s-Pd1.5%
TiO2 s-Au1.5%
TiO2 s-Pt1.5%
TiO2 s
a.u.
20
30
40
50
60
70
2θ

Figure 2

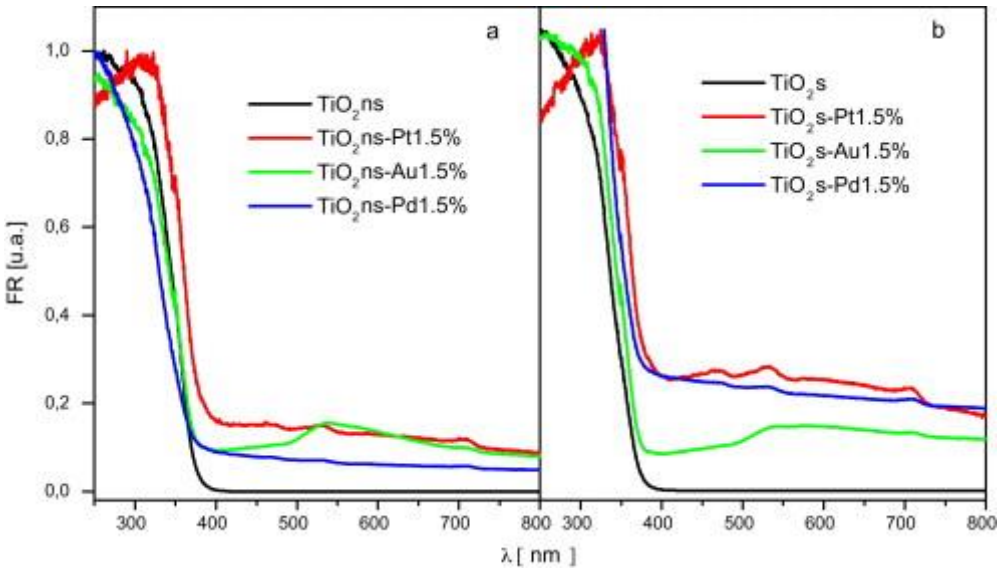
a
b
TiO2ns
TiO2ns-Pt1.5%
TiO2ns-Au1.5%
TiO2ns-Pd1.5%
TiO2s
TiO2s-Pt1.5%
TiO2s-Au1.5%
TiO2s-Pd1.5%
FR [u.a.]
λ [nm]
1,0
0,8
0,6
0,4
0,2
0,0
300
400
500
600
700
800

Figure 3

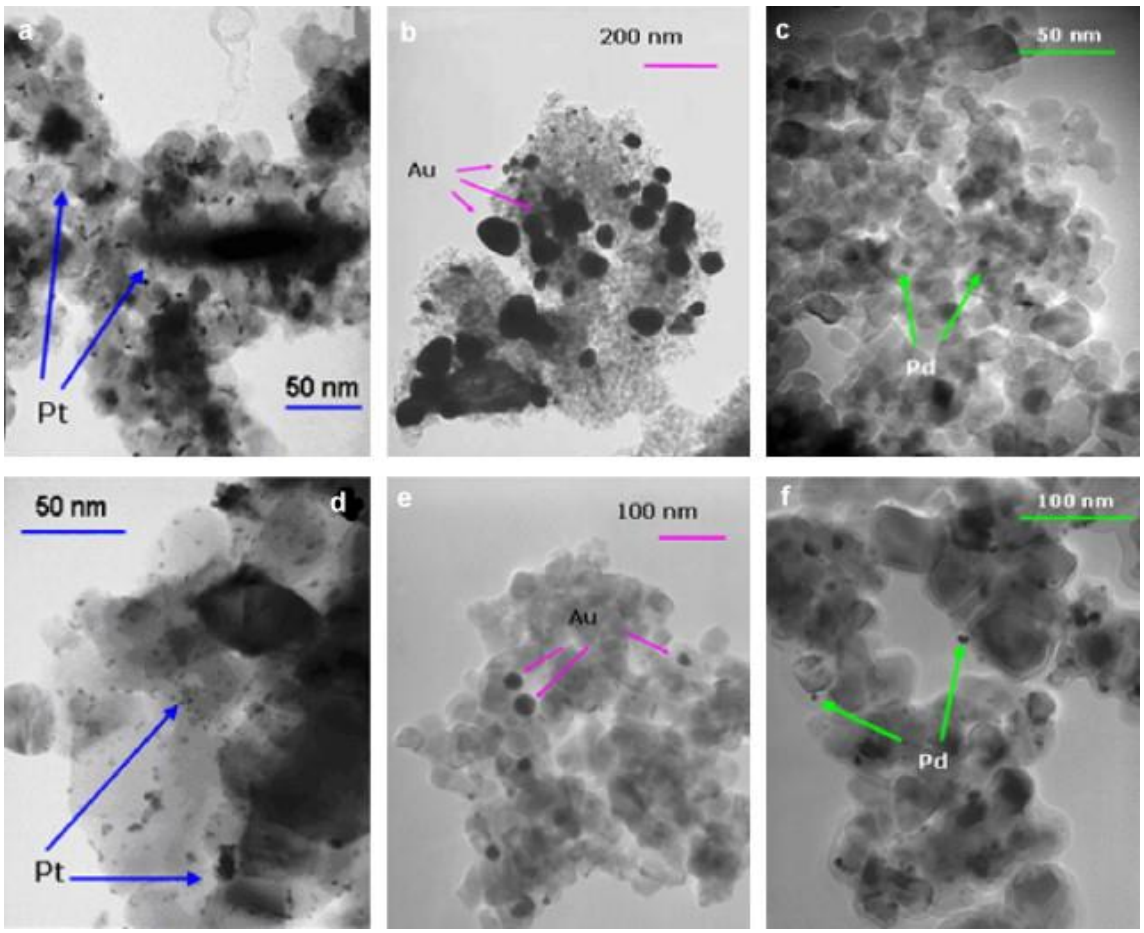

Figure 4

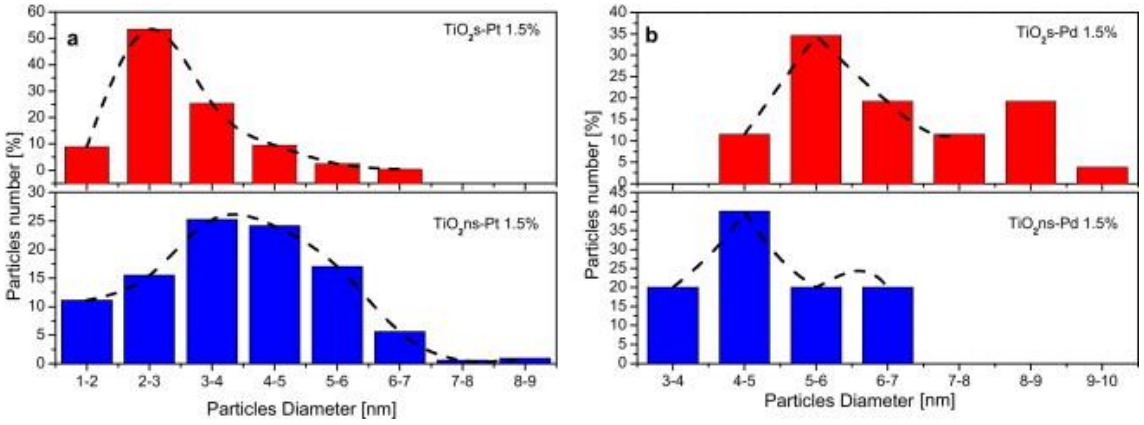
a
TiO2s-Pt 1.5%
TiO2ns-Pt 1.5%
Particles number [%]
Particles Diameter [nm]
1-2
2-3
3-4
4-5
5-6
6-7
7-8
8-9
b
TiO2s-Pd 1.5%
TiO2ns-Pd 1.5%
Particles number [%]
Particles Diameter [nm]
3-4
4-5
5-6
6-7
7-8
8-9
9-10

Figure 5

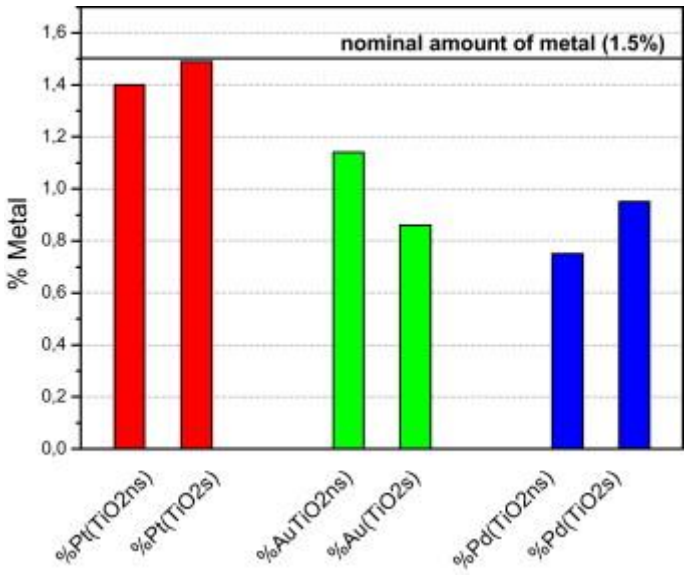
nominal amount of metal (1.5%)
% Metal
1,6
1,4
1,2
1,0
0,8
0,6
0,4
0,2
0,0
%Pt(TiO2ns)
%Pt(TiO2s)
%AuTiO2ns)
%Au(TiO2s)
%Pd(TiO2ns)
%Pd(TiO2s)

Figure 6

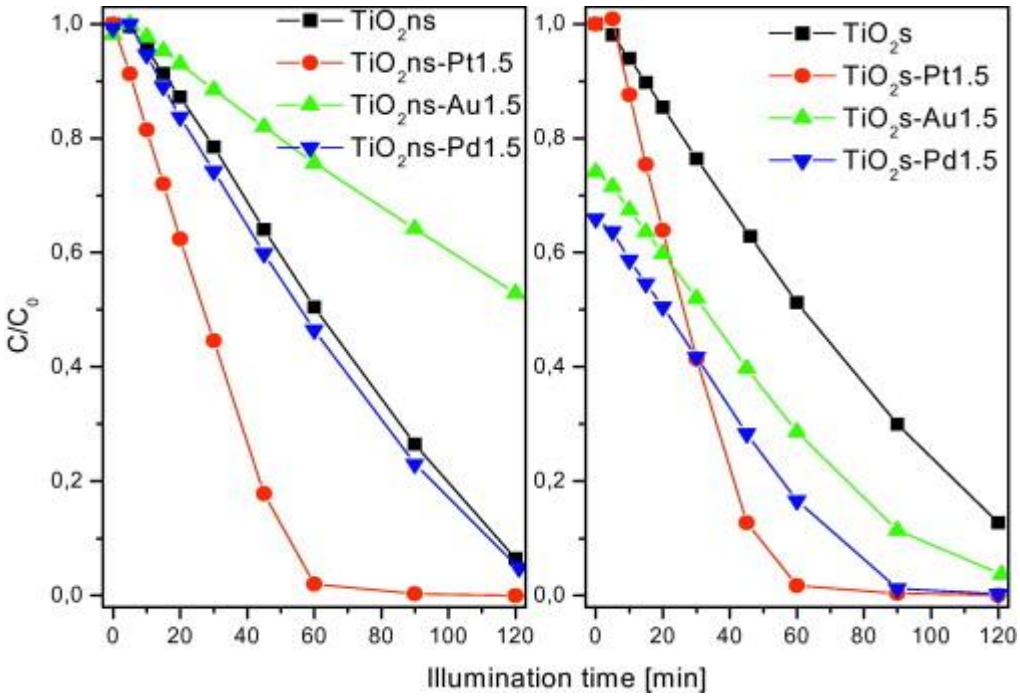
TiO2ns
TiO2ns-Pt1.5
TiO2ns-Au1.5
TiO2ns-Pd1.5
TiO2s
TiO2s-Pt1.5
TiO2s-Au1.5
TiO2s-Pd1.5
C/C0
Illumination time [min]
0,0
0,2
0,4
0,6
0,8
1,0
0
20
40
60
80
100
120

Figure 7

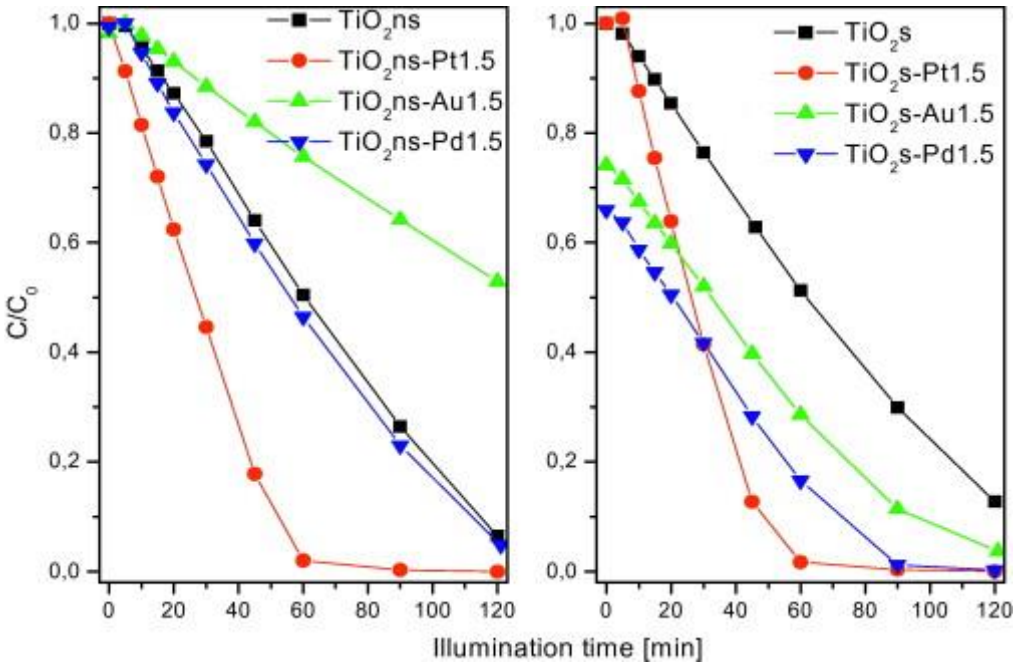
TiO2ns
TiO2ns-Pt1.5
TiO2ns-Au1.5
TiO2ns-Pd1.5
TiO2s
TiO2s-Pt1.5
TiO2s-Au1.5
TiO2s-Pd1.5
C/C0
Illumination time [min]
0,0
0,2
0,4
0,6
0,8
1,0
0
20
40
60
80
100
120

Figure 8

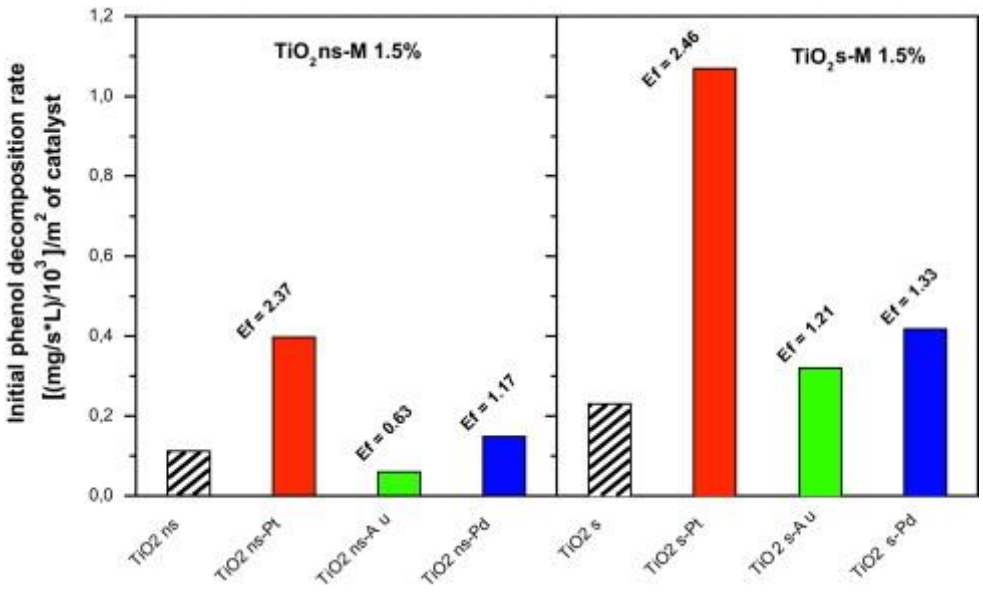
Initial phenol decomposition rate
[(mg/s*L)/10^3]/m^2 of catalyst
1,2
1,0
0,8
0,6
0,4
0,2
0,0
TiO2 ns-M 1.5%
TiO2 s-M 1.5%
Ef = 2.37
Ef = 0.63
Ef = 1.17
Ef = 2.46
Ef = 1.21
Ef = 1.33
TiO2 ns
TiO2 ns-Pt
TiO2 ns-A u
TiO2 ns-Pd
TiO2 s
TiO2 s-Pt
TiO2 s-A u
TiO2 s-Pd